THE JOURNAL OF PHYSICAL CHEMISTRY B

ARTICLE

pubs.acs.org/JPCB

Calorimetric Study of Water's Glass Transition in Nanoscale Confinement, Suggesting a Value of 210 K for Bulk Water

Masaharu Oguni,*[,†] Yasuhiro Kanke,[†] Atsushi Nagoe,[†] and Seitarô Namba[‡]

[†]Department of Chemistry, Graduate School of Science and Engineering, Tokyo Institute of Technology, 2-12-1 O-okayama, Meguro-ku, Tokyo 152-8551, Japan

[‡]Institute for Nanoscience & Nanotechnology, Waseda University, 513 Wasedatsurumaki-cho, Shinjuku-ku, Tokyo 162-0041, Japan

ABSTRACT: At what temperature between 136 and 165 K the glass transition of water occurs is still controversial, while the crystallization of water prevents the determination. To confine water in nanopores stabilizes its liquid state down to low temperatures. Heat capacities and enthalpy relaxation effects of the water confined within MCM-41 nanopores with diameters in the range 1.5−5.0 nm were measured in this work by using adiabatic calorimetry. No fusion of the confined water was detected up to 2.0 nm, part of the water exhibited fusion in 2.1 nm pores, and the whole internal water which excludes the molecules interacting with the pore-wall atoms crystallized within pores with diameter of 2.3 nm and above. A glass transition of the internal water occurred at a temperature T_g = 160−165 K for pore diameters in the range 1.5−2.0 nm and at 205−210 K for diameters of 2.0 and 2.1 nm; thus, the T_g jumped from 165 to 205 K at 2.0 nm. The jump is connected to the development of hydrogen-bond network to a more complete one as the diameter is increased, and is conjectured as caused by the increase in the number, from three to four, of hydrogen bonds formed by each molecule. These imply that the glass transition of bulk water occurs at 210 K, which is much higher than 136 or 165 K debated so far.

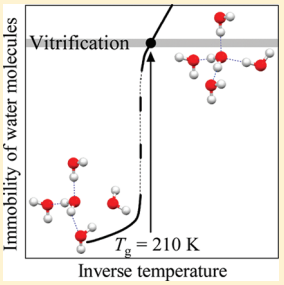

1. INTRODUCTION

When cooled without crystallization, many liquids pass through an equilibrium supercooled state to a nonequilibrium glassy state.[1−5] Above the glass transition temperature, T_g, the positions and orientations of molecules vary on a short time scale, whereas below T_g they become fixed on an experimental time scale. However, unlike many such liquids, it is difficult to prevent water from crystallizing; even emulsified water crystallizes at 235 K on cooling,[3−6] and amorphous solid water (ASW), which can be prepared by vapor deposition at very low temperatures, crystallizes at 150 K on heating.[7−9] Accordingly, liquid or glassy bulk water has not been realized between 150 and 235 K,[10] as makes it impossible to directly probe the thermodynamic and kinetic properties of liquid water in this temperature range.[2−5] This situation has left unclear what the T_g of water is. Since a heat-capacity jump was observed on heating before the vapor-deposited ASW crystallized,[7] T_g = 136 K has been claimed as a candidate for both ASW[8] and hyperquenched glassy water (HGW).[11−13] Low-density amorphous (LDA) solid water has also been reported to exhibit a T_g of 129 K.[14] However, the transition signal is weak, probably due to the nonequilibrium character of those amorphous materials even above 136 K.[8,9,11−16] On the other hand, T_g = 165 K has been proposed based on the temperature dependence of the heat release of HGW.[17] The self-diffusivity of ASW below 160 K has been also reported[18] to be significantly smaller than the value expected assuming that T_g = 136 K. This supports that the glass transition occurs above 160 K. Thus, the T_g of water is still controversial between 136 and 165 K.[8,9,11−18] The resolution is important for understanding both the low-temperature structure of water and the glass-transition mechanism.

Reducing the sample size increases the stability of the liquid relative to that of the crystal. One can imagine what occurs when the pore diameter is extremely small and is then gradually increased. In the smallest limit, only one molecule is enclosed along the pore diameter and no characteristics associated with an aggregate of water molecules appear since its arrangement is completely dominated by the pore wall structure. As the pore size is increased, the characteristics of liquid water as a molecular aggregate start to appear. Initially, the liquid state is more stable than the crystalline state even at low temperatures, though it is uncertain whether the structure and properties of this water correspond with those of bulk water. In fact, a lot of nanopore water systems are known to remain in the noncrystalline state at low temperatures ubiquitously on earth. As long-range molecular interactions commence to operate in aggregations, the crystalline state will become increasingly stable.[19−24] In this sense, what the T_g of water is also concerns the low-temperature behaviors of nanopore water in biology, geology, and other fields.

In a previous study using silica-gel nanopores,[24,25] we found that the interfacial water molecules that interact with siloxane and silanol groups on the pore wall do not crystallize and exhibit a glass transition at 115−125 K depending on the pore size.

Special Issue: H. Eugene Stanley Festschrift

Received: April 12, 2011
Revised: August 6, 2011
Published: August 19, 2011

ACS Publications © 2011 American Chemical Society

In addition, the internal water molecules that interact only with other water molecules were found to remain in the liquid state with a glass transition at 160 K in pores with diameters up to about 2 nm and to crystallize into ice above 2 nm.[24] A detailed diameter dependence of the thermal properties could not be determined because of the rather broad pore-size distribution present in silica gel and due to the distortion of the pore shapes from cylinders. The result, however, reveals that executing the calorimetric work as a function of the precise diameter is indispensable for determining the thermal and kinetic properties of water between 150 and 235 K. Characteristics close to those of bulk water are potentially realized in pores having a diameter close to the one at which crystallization occurs, namely near the critical diameter of 2.0 nm. This view is further supported by the result of the computer simulation of the room-temperature water confined in infinite hydrophilic silica surfaces with a separation distance d between 0.6 and 5.0 nm: It was reported that the in-plane local translational dynamics are independent of the confinement length scale in the range $d \geq 1.0$ nm, and the region of surface-dominated slowing down in the dynamics extends up to ca. 1.0 nm away from the surfaces.[26]

In this study,[27] the thermodynamic and kinetic properties of confined water were investigated using an adiabatic calorimeter[27] and porous silica MCM-41 with average pore diameters in the range of 1.5−5.0 nm. The pore-diameter dependence was examined especially in detail around 2.0 nm, although a distribution of the pore diameters is still existent in each porous silica; the distribution is, for example, ca. 0.3 nm in the full width at half-maximum around the average diameter of 2.0 nm. The presence of a glass transition was confirmed by observing systematic spontaneous enthalpy-relaxation effects of the samples cooled rapidly or slowly prior to performing heat capacity measurements. The glass transition of the interfacial water molecules was found to occur in the range 114−122 K, and that of the internal water molecules occurred at 160−165 K for pore diameters in the range 1.5−2.0 nm and at 205−210 K for pore diameters in the range 2.0−2.1 nm; thus, the T_g jumped from 165 to 205 K at a pore diameter of 2.0 nm.

2. METHOD FOR DETERMINING THE PRESENCE OF A GLASS TRANSITION BY ADIABATIC CALORIMETRY

Determination of heat capacities by using adiabatic calorimetry is executed by an intermittent heating method:[28] The initial temperature T_i is determined by following the temperature in a thermometry period. An electrical energy of ΔE is supplied to the cell producing a temperature rise ΔT, and then the final temperature T_f is determined by following again the temperature in the next thermometry period. The temperature rise is calculated as $\Delta T = T_f - T_i$, and the gross heat capacity of the cell is evaluated as $C_{gross} = \Delta E/\Delta T$. The heat capacity of the sample is estimated by subtracting the heat capacity of the empty cell from that of the cell containing the sample. When the sample exhibits spontaneous heat-release or -absorption effects due to a glass transition, these effects are observed as a temperature rise or fall (dT/dt), respectively, of the calorimeter cell during the thermometry. The relaxation rates of the molar enthalpy of the sample are then evaluated using $(dH_m/dt) = -C_{gross}(dT/dt)/n$, where n is the quantity of the sample.

Figure 1 illustrates how a glass transition is observed by the adiabatic calorimetry. The upper portion schematically shows the trace followed by the sample on the enthalpy vs temperature surface. The dashed line represents the equilibrium enthalpy curve. In (a), the sample is rapidly cooled typically at about 10 K min^{-1} from above T_g to below T_g. Then, the heat capacities and enthalpy relaxation rates of the sample are measured by repeating the thermometry and energy supply, as stated above, typically at an average heating speed of about 0.1 K min^{-1}. At low temperatures, the relaxation time is long compared with the experimental time scale so that no appreciable relaxation effects should be observed. As the temperature increases, since the sample's enthalpy is higher than the equilibrium enthalpy, a heat-release effect starts to be observed during the thermometry, as indicated by the nearly vertical segments. The nearly horizontal segments indicate the temperature rise due to the energy supply. After the enthalpy of the sample crosses the equilibrium curve, it becomes lower than the equilibrium enthalpy and the sample commences to exhibit a heat-absorption effect. The temperature dependence of the enthalpy relaxation rates is plotted schematically with the filled circles labeled (a) in the lower portion of Figure 1. On the other hand, in (b) of the upper portion, the sample is slowly cooled typically at about 10 mK min^{-1} (20 mK min^{-1} in this study) from above to below T_g. As the temperature increases from the lower side, a heat release effect is hardly observed because the relaxation time is sufficiently long in the range where the enthalpy exceeds the equilibrium enthalpy, and then the heat-absorption effect starts to be observed as indicated

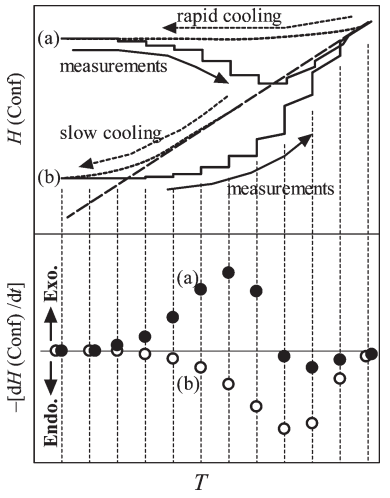

Figure 1. Calorimetric determination of the presence of a glass transition: Enthalpic path (upper portion) followed by a sample in the transition region, and temperature dependence of the rates (lower portion) of spontaneous enthalpy-relaxation drifts accompanied with the transition. The dashed line in the upper portion represents the equilibrium enthalpy curve. When the sample is cooled (indicated by the dotted line and arrow) rapidly or slowly, the enthalpy of the sample deviates from the dashed line at higher or lower temperatures due to the lengthening of the equilibration time relative to the cooling speed and is maintained in the respective nonequilibrium states (a) or (b). The temperature of the sample is then increased (indicated by the solid line and arrow) for measurements by an intermittently heating method with repeated thermometry and energy supply to the calorimeter cell. The sample starts to release or absorb heat to approach the equilibrium enthalpy at each temperature in the glass transition region. The release/absorption rates as a function of temperature are indicated by the symbols ● or ○ in the lower portion of the figure for the rapidly or slowly precooled samples, respectively. The presence of a calorimetric glass transition is determined by observing such a set of systematic enthalpy relaxation effects for the samples precooled at different speeds.

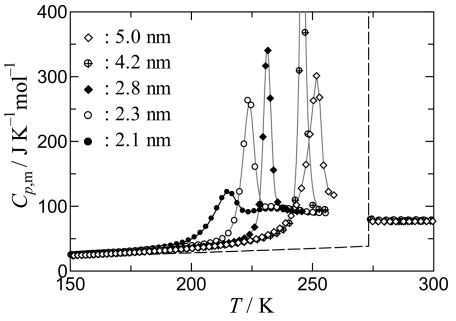

Figure 2. Molar heat capacities showing the effect of ice fusion in the pores with diameters in a range 2.1−5.0 nm. The dashed line represents the dependence of bulk water and ice.[32]

by the almost vertical segments. The absorption (negative −dH/dt) effects (indicated by the open circles labeled (b) in the lower portion of the figure) increase gradually in rate, reach a maximum, and then approach normal behavior without appreciable drift during the thermometry. Therefore, the presence of a glass transition can be determined by observing such systematic enthalpy-relaxation effects for the samples subject to the precooling at different speeds, as shown in the lower portion of Figure 1. The temperature at which the absorption rate reaches its maximum in the slowly precooled sample empirically corresponds to the T_g at which the relaxation time τ becomes 1 ks.[28,29]

3. EXPERIMENTAL SECTION

Silica MCM-41 was synthesized according to the previously described procedure.[30] The pore diameter distribution was determined using a Japan Bell porosimeter of type Mini and by the BJH method.[31] Degassed water was introduced into the silica pores on a glass vacuum line; the introduction was easily done under vacuum on account of the partially hydrophilic nature of the pore wall with silanol groups. The volume of the water used exceeded the pore volume to ensure that there were no voids in the pores. The sample with the excess water was loaded into a calorimeter cell in an atmosphere of helium gas.

Heat capacities were measured using an adiabatic calorimeter. Calorimetry was conducted by the intermittent heating method as stated in the preceding section.[28] The heat capacity of the water within the pores was derived by subtracting, from the heat capacity of the sample, the contributions of the excess bulk ice/water and of the MCM-41; the former contribution was estimated by evaluating the quantity of the bulk ice/water from the directly measured enthalpy of fusion at 273 K and utilizing the literature data of heat capacities of ice/water[32] and the latter one by directly measuring the heat capacities of dry MCM-41. Finally, the molar heat capacity was calculated by dividing the obtained values by the quantity n of the pore water used.

4. RESULTS AND DISCUSSION

4.1. Heat Capacity. Figure 2 shows the experimentally derived heat capacities of water and ice confined within pores with diameters in the range 2.1−5.0 nm. The dashed line in the figure represents the heat capacity curve of bulk ice and water.[32] There is no data plotted in the range 250−273 K because the fusion of the extra bulk water outside the MCM-41 particles prevented the heat capacity of the pore water from being accurately determined. Interfacial water molecules on the pore wall did not crystallize; the

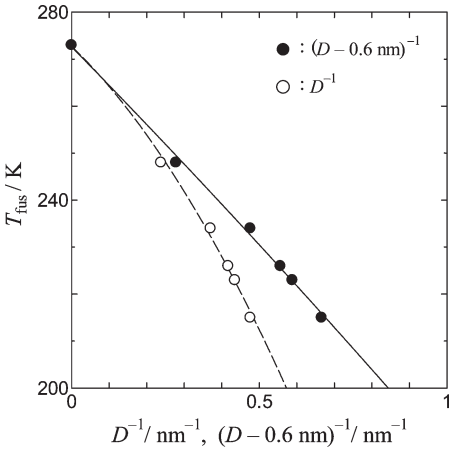

Figure 3. Linearity test of the fusion temperature against the inverse of the diameter for the ice formed in the center of nanopores: ○, the abscissa is taken as the inverse of the measured pore diameter D; ●, the abscissa is taken as the inverse of $(D - 0.6\ \mathrm{nm})$. A linear relation is derived when 0.6 nm is subtracted from the diameter. The interfacial water molecules, with an average layer thickness of 0.3 nm, are indicated to interact with siloxane or silanol groups on the pore wall and to be in a noncrystalline state even when the water molecules in the pore center have crystallized into ice.

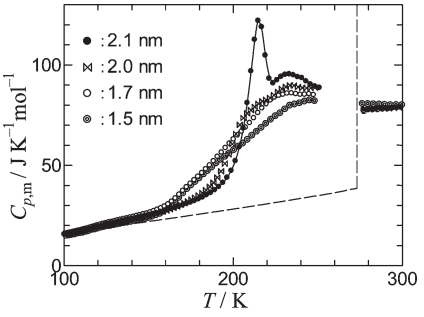

Figure 4. Comparison of the molar heat capacities, showing their rise due to glass transitions at different temperatures, of the water in the pores with diameters in the range 1.5−2.1 nm. The dashed line represents the dependence of bulk water and ice.[32] No fusion was observed in the water for pore diameters below and of 2.0 nm, and only part of the water in 2.1 nm diameter pores showed its fusion with the heat capacity peak at 214.8 K. The heat capacities jump remarkably in the range 160−170 K for 1.5 and 1.7 nm diameter pores and in the range 200−210 K for 2.0 and 2.1 nm diameter pores.

reasons for this are discussed below. All of the internal water crystallized on cooling, forming ice for pore diameters above 2.3 nm, and exhibited a large peak in the heat capacity curve on heating due to fusion of the ice formed. In 2.1 nm diameter pores, only part of the water crystallized as seen by a small peak at 214.8 K, and the other remained liquid down to the lowest temperature measured.

Fusion temperatures T_{fus} (taken to be the peak temperatures) are plotted in Figure 3 as a function of the inverse of the diameter. The open and filled circles represent the data points obtained when the measured pore diameter D was used as the diameter and when $(D - 0.6\ \mathrm{nm})$ was used as the diameter, respectively.

The linear relation obtained in the latter case agrees with the prediction of Gibbs and Thomson.[33] A value of 0.6 nm is considered to be the size occupied by interfacial water, which

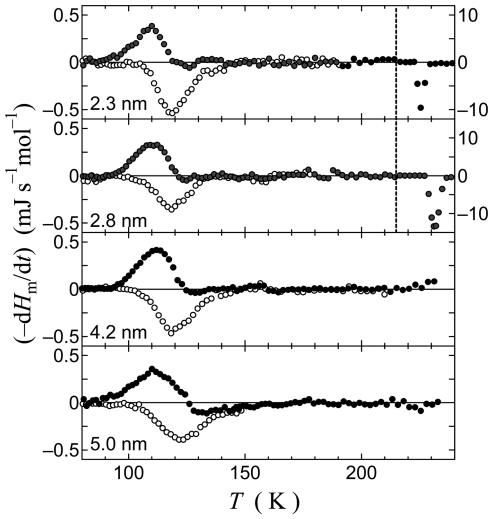

Figure 5. Rates of the spontaneous enthalpy release and absorption accompanied with a glass transition of the interfacial water and fusion of the internal water in the pores with diameters 2.3−5.0 nm: ●, sample cooled rapidly at around 10 K min^{-1} prior to the measurements; ○, sample cooled slowly at around 20 mK min^{-1}. The pore diameter is written within each panel. Note that the ordinate scales for 2.3 and 2.8 nm pores are different between the temperature ranges below and above 215 K. The exothermic (positive $-dH_m/dt$) and endothermic (negative $-dH_m/dt$) effects for rapidly and slowly precooled samples respectively are characteristic of a glass transition as described in Figure 1 and associatively in the text. The interfacial water molecules interacting with the silanol groups of pore wall are evidenced to be in the noncrystalline state as the glass transition originates from the freezing-in of their rearrangement motion, while the internal water molecules being in the crystalline state do not undergo their rearrangement. The transition temperature T_g, determined as the point at which the heat absorption rate for the slowly precooled sample reveals its maximum,[28,29] lies in the range 118−122 K. The enthalpy absorption effects around 224 K for 2.3 nm pores and 232 K for 2.8 nm pores, showing sharp peaks, are ascribed to fusion of the internal water within the pores.

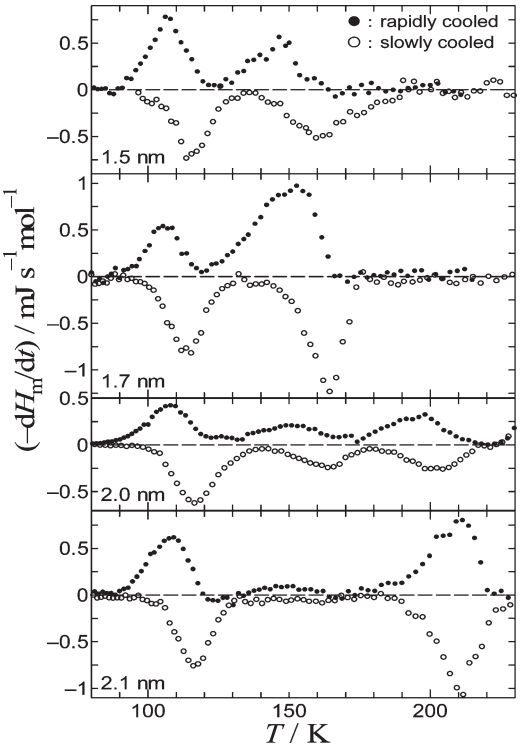

Figure 6. Plots of the rates of the spontaneous enthalpy release and absorption due to glass transitions of the internal water in the pores with diameters 1.5−2.1 nm, demonstrating that the glass transition of water occurs at 210 K within the nanopores with the limiting diameter at which the water commences to crystallize into ice: ●, sample precooled rapidly at around 10 K min^{-1}; ○, sample precooled slowly at 20 mK min^{-1}. Systematic sets of spontaneous enthalpy relaxation rates indicate that the glass transitions appear in three different temperature ranges. The T_g of the interfacial water lies in the range 114−117 K smoothly connected with the values for 2.3−5.0 nm diameter pores (see Figure 5), and that of the internal water is determined as 160 K for 1.5 nm, 165 K for 1.7 nm, 165 and 205 K for 2.0 nm, and 210 K for 2.1 nm diameter pores. The T_g of the internal water is concluded to increase stepwise from 165 to 205 K at 2.0 nm with increasing the pore diameter and to be 210 K at 2.1 nm at which the crystallization of the water starts.

is twice the thickness of the interfacial water layer. The thickness of 0.3 nm is in reasonable agreement with estimates (0.3−0.4 nm) of the interfacial layer thickness obtained by other research groups.[19,22] Since a water molecule has a van der Waals diameter of about 0.4 nm, this thickness indicates that the interfacial water layer consists of only a single layer of water molecules on average.

Figure 4 shows the experimentally derived heat capacities for diameters in the range 1.5−2.1 nm. The dashed line represents the heat capacity curve of bulk ice and water.[31] No fusion of ice was observed in 1.5−2.0 nm diameter pores. Heat capacities increase appreciably around 160−170 K in 1.5 and 1.7 nm diameter pores and around 200−210 K in 2.0 and 2.1 nm diameter pores.

4.2. Spontaneous Enthalpy Relaxation as Evidencing the Presence of a Glass Transition. Figure 5 shows the rates of spontaneous heat-release and -absorption observed, on heating, in the thermometry periods of the heat-capacity measurements of the water confined within pores with diameter of 2.3, 2.8, 4.2, and 5.0 nm. The filled and open circles represent the results of samples rapidly precooled at about 10 K min^{-1} and slowly precooled at about 20 mK min^{-1}, respectively, to the lowest temperature before the heat-capacity measurements. A systematic set of heat-release and -absorption effects was observed in the temperature range 100−130 K, indicating the presence of a glass transition. The T_g at which the relaxation time τ becomes 1 ks was estimated to be approximately 118 K for 2.3 nm diameter pores and about 122 K for 5.0 nm diameter pores; thus, it rises slightly with increasing diameter. This diameter dependence indicates that the glass transition occurs in pore water. Since, as mentioned above, the internal water is essentially in the crystalline state, the glass transition is concluded to originate from the freezing-in of the rearrangement motion of interfacial water molecules.[34] The heat-absorption effects with sharp peaks observed around 224 K for 2.3 nm pores and 232 K for 2.8 nm pores in Figure 5 are ascribed to fusion of the ice formed in the pore center.

Figure 6 shows the results of the rates of spontaneous enthalpy relaxation due to water in 1.5, 1.7, 2.0, and 2.1 nm diameter pores. Glass transitions were found to occur in three temperature regions. The first glass transition occurred at 114−117 K; the pore-diameter dependence of the transition temperature is connected smoothly to the results for the water in 2.3−5.0 nm diameter pores. This transition originates from the freezing-in of

the rearrangement of the interfacial water molecules interacting with siloxane or silanol groups on the pore wall of MCM-41.[34] The second glass transition was observed for pore diameters between 1.5 and 2.0 nm, and the third one for pores with diameters of 2.0 and 2.1 nm. Since no glass transitions were detected in these two temperature regions in 2.3−5.0 nm diameter pores in which the internal water crystallized, these two glass transitions are attributed to freezing-in of the rearrangement of the internal water molecules that remain in the liquid state without crystallizing. The internal water in 1.5 and 1.7 nm diameter pores exhibited only the second glass transition. The magnitude of the heat-release and -absorption effects, namely the relaxation strength, increased with increasing the diameter due to the increase in the proportion of internal water to interfacial water. Associated with the relaxation effects, there is a heat-capacity rise at around 160−170 K; this rise is a little larger in the 1.7 nm diameter pores than in the 1.5 nm pores (see Figure 4). When the pore diameter was further increased to 2.0 nm, the heat-release and -absorption effects of the second glass transition decreased and the third glass transition appeared. In the case of the 2.1 nm diameter pores, the effects of the third glass transition are very large while those of the second glass transition are negligibly small. These results demonstrate that the T_g of the water located in the center of the pores increases in a stepwise manner with increasing pore diameter. The T_g of the second glass transition was estimated to be 160 K for 1.5 nm diameter pores and 165 K for 1.7 and 2.0 nm diameter pores, and the T_g of the third glass transition was estimated to be 205 K for 2.0 nm diameter pores and 210 K for 2.1 nm diameter pores.

Because the interfacial water molecules form hydrogen bonds with the firmly fixed and randomly located silanol groups and are affected by the repulsive/attractive interactions with the irregularly arranged siloxane groups, these water molecules are considered to be rather restricted in their positions and to form an incomplete network of hydrogen bonds. Consequently, when the diameter of the internal water is relatively small, the internal water molecules will also form a comparatively incomplete hydrogen-bond network.[26] The incompleteness originates from the circumstance that some of the internal water molecules should form hydrogen bonds with the interfacial water molecules. The T_g of 165 K is considered to be correlated with such circumstances. This consideration leads to the conclusion that the jump in the T_g from 165 to 210 K reflects the formation of a tetrahedrally connected hydrogen-bond network due to increase in the number of internal water molecules associated with the increase in the pore diameter. On the other hand, the network formation stabilizes the crystalline phase at low temperatures, as indicated by the appearance of fusion of the ice partially formed in the pores with average diameter of 2.1 nm (see Figures 2 and 4).

One might think that the enthalpy relaxation effects around 210 K are connected with the heat capacity peak at 214.8 K for 2.1 nm diameter pore water.[35] Experimentally, the same heat-capacity peak was obtained for the samples precooled rapidly or slowly through the 210 K region. In addition, no heat-capacity peak was detected in 2.0 nm pore water (see Figure 4), while the water exhibited the same systematic enthalpy relaxation effects around 210 K as did within the 2.1 nm pores (see Figure 6). These facts demonstrate that the enthalpy relaxation effects around 210 K and the heat capacity peak at 214.8 K for the 2.1 nm pore water are unrelated phenomena that are caused by different mechanisms. As mentioned above, the heat capacity peak at 214.8 K is attributed to the fusion of the ice formed in the center of pores with a little larger diameter than 2.1 nm. Even though MCM-41 was used instead of silica gel, it still has a certain pore diameter distribution, which accounts for why the two above-mentioned independent phenomena are observed in the 2.1 nm pores. These results conversely indicate that the pore with diameter of 2.1 nm provides the limit at which the confined internal water can remain in the liquid state.

4.3. Physical Meaning of the T_g Jump. It is worth considering what the T_g values of 115, 165, and 210 K mean physically. Since the relaxation time τ in isostructural conditions follows an Arrhenius expression, $\tau = \tau_0 \exp(\Delta\varepsilon_a/RT)$,[36−38] the activation energy $\Delta\varepsilon_a$ can be expressed in terms of T_g by $\Delta\varepsilon_a = 2.3RT_g \log(\tau/\tau_0)$, where R is the gas constant and the pre-exponential factor τ_0 has been found to be of the order of 10^{-14} s in many systems.[28,37,38] Substituting $\tau = 1$ ks and $T_g = 115$, 165, and 210 K yields $\Delta\varepsilon_a$ = 37, 54, and 68 kJ mol^{-1}, respectively. As the hydrogen-bond energy of the O−H···O bond with O····O length of 0.27−0.28 nm is known to be 15−20 kJ mol^{-1}, $\Delta\varepsilon_a$ = 37, 54, and 68 kJ mol^{-1} are approximately equivalent to the energies required to break two, three, and four hydrogen bonds, respectively. It is currently unclear whether the activation process actually involves breaking these numbers of hydrogen bonds. However, in view that such discrete increase in T_g with the change in pore size has never been observed in other van der Waals liquids, it is certain that the discreteness in the change of the activation energy is correlated with the hydrogen-bond network structure formed in water and therefore the number of hydrogen bonds broken. In fact, it has been found by a structural study that the number of hydrogen bonds increases as the pore size increases in the nanometer range.[39]

4.4. Prediction of T_g for Bulk Water and Implication of the T_g Value Predicted. Bulk water corresponds to the internal water in large diameter pores. The glass transition of water molecules occurs at discretely increasing temperatures of 115, 165, and 210 K with increasing pore size. Considering that the magnitudes of the T_g jumps are about 50 K, the next higher glass transition temperature is expected to be about 260 K. Since bulk water is in the equilibrium supercooled liquid state down to 235 K, its T_g must be lower than 235 K. Thus, the T_g of bulk water is concluded to be 210 K. This conclusion is reasonable because partial crystallization occurred in 2.1 nm diameter pores within which all of the internal water had formed a structure having the T_g = 210 K; namely, the internal water in 2.1 nm diameter pores and at 210 K has a structure that easily induces the formation of ice. Thus, the water is expected to have the same liquid structure with well-developed hydrogen-bond network as bulk water has. The T_g = 210 K is much higher than the values 136 or 165 K debated so far.[8,9,11−18,24,25]

Based on the implication that bulk water undergoes the glass transition at T_g = 210 K, it is attractive to consider temperature dependence of the relaxation times of bulk water. The relaxation time is 10^3 s at 210 K by the definition of a calorimetric glass transition. On the other hand, the relaxation times around 240 K are known to be on the order of 10^{-11} s, as evaluated from the viscosity η data.[3,37,40] These mean that the relaxation times must increase dramatically with reducing temperature in a narrow temperature range between 240 and 210 K. Further, as stated above, T_g = 210 K is considered as corresponding to the $\Delta\varepsilon_a$ for breaking four hydrogen bonds in the rearrangement of a water molecule. Four is the upper limit, because it is difficult to conceive that a water molecule forms and simultaneously breaks five or six ordered hydrogen bonds for its rearrangement; thus,

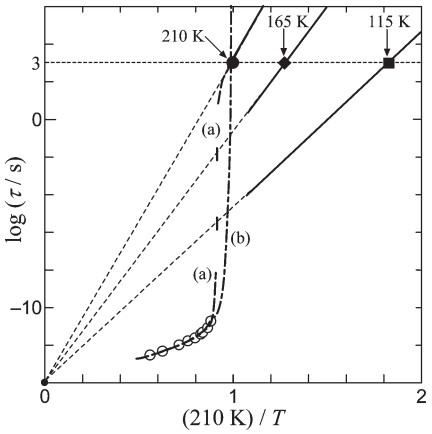

Figure 7. Potential temperature dependence of relaxation times presented as an Arrhenius plot, with the inverse temperature normalized by 210 K, for the rearrangement processes of pore- and bulk-water molecules: ○, deduced from the viscosity data of bulk water;[3,40] ●, ♦, and ■, T_g's observed in the present study. The three solid lines are the expected dependences, which exhibit Arrhenius behaviors even above T_g due to the presence of a pore-wall effect. T_g of bulk water is implied to be 210 K, as stated in text. The dashed line labeled (a) represents the dependence predicted in the case where the relaxation times of bulk water exhibit a change from fragile to strong behavior on cooling; there, the activation energy and therefore the relaxation time take discrete jumps in the low-temperature situation with highly developed hydrogen-bond network, as rationalized in section 4.3. The dot-dashed line labeled (b) represents the dependence predicted in the case where the relaxation times follow the Vogel−Fulcher law.

the corresponding value of $\Delta\varepsilon_a$ is also an upper limit. Bulk water at 210 K then forms potentially a considerably developed hydrogen-bond network, and the limitation nature of $\Delta\varepsilon_a$ is expected to bring the relaxation times to exhibit an Arrhenius behavior immediately above 210 K. As a consequence, it is reasonable to consider that the relaxation times increase dramatically between 240 and 210 K and reveal simultaneously a change from fragile to strong behavior on cooling, as shown in Figure 7. The former dramatic increase is reasonably expected to occur around 233 K where the heat capacities show their maximum and therefore the hydrogen-bond network develops remarkably.[41−43] This expectation is consistent with the recent reports that the negative volume expansion coefficient and so on of the water in pores show their maxima around 233 K.[4,44] The latter fragile-to-strong change in water has been also predicted to occur,[45,46] and its experimental verification has been tried.[47]

5. CONCLUSIONS

In the present study, we found that the glass transition of water within MCM-41 nanopores occurs at discretely increasing temperatures of 115, 165, and 210 K with increasing pore diameter. This is a characteristic of water and probably of other related liquids such as silicon dioxide, but it has never been observed in simple van der Waals liquids. The characteristic is connected to the fact that the water molecules aggregate through forming a hydrogen-bond network. It is therefore suggested that the activation energy for the rearrangement of a molecule must be correlated with the number of hydrogen bonds to be broken in the activation process.

Bulk water properties may just appear at a pore diameter of 2.1 nm where crystallization inevitably proceeds. Based on this, we concluded that the T_g of bulk water is 210 K. This value is recognized as the highest T_g that a water molecule can take, since each molecule forms four bonds in a relatively developed hydrogen-bond network. The relaxation times are expected to have Arrhenius temperature dependence in the region just above 210 K, and thus must undergo a change from fragile to strong behavior between 240 and 210 K. These are intriguing to be further verified by any experimental contrivances in future, and also it should be elucidated why ASW, HGW, and LDA potentially show some weak anomalous signal around 136 K and crystallize at 150 K much below the T_g = 210 K.

These considerations imply that, in general, the elementary freezing-in process as the mechanism responsible for glass transitions is essentially the rearrangement process changing the position and orientation of each molecule in liquids and glasses.[37] This implication for the mechanism is a profound claim also to be investigated in the future in detail.

AUTHOR INFORMATION

Corresponding Author

*E-mail: moguni@chem.titech.ac.jp.

ACKNOWLEDGMENT

This work was financially supported partly by Grants-in-Aid for Scientific Research (Grants 18350003 and 21340118) from the Ministry of Education, Culture, Sports, Science, and Technology, Japan.

REFERENCES

(1) Ediger, M. D.; Angell, C. A.; Nagel, S. R. *J. Phys. Chem.* **1996**, *100*, 13200–13212.
(2) Debenedetti, P. G. *J. Phys.: Condens. Matter* **2003**, *15*, R1669–R1726.
(3) Angell, C. A. In *Water Comprehensive Treatise*; Franks, F., Ed.; Plenum: New York, 1982; Vol. 7, pp 1−81.
(4) Angell, C. A. *Chem. Rev.* **2002**, *102*, 2627–2649.
(5) Angell, C. A. *Science* **2008**, *319*, 582–587.
(6) Angell, C. A.; Oguni, M.; Shichina, W. J. *J. Phys. Chem.* **1982**, *86*, 998–1002.
(7) McMillan, J. A.; Los, S. C. *Nature* **1965**, *206*, 806–807.
(8) Hallbrucker, A.; Mayer, E.; Johari, G. P. *J. Phys. Chem.* **1989**, *93*, 4986–4990.
(9) MacFarlane, D.; Angell, C. A. *J. Phys. Chem.* **1984**, *88*, 759–762.
(10) Mishima, O.; Stanley, H. E. *Nature* **1998**, *396*, 329–335.
(11) Johari, G. P.; Hallbrucker, A.; Mayer, E. *Nature* **1987**, *330*, 552–553.
(12) Johari, G. P.; Hallbrucker, A.; Mayer, E. *Science* **1996**, *273*, 90–92.
(13) Smith, R. S.; Kay, B. D. *Nature* **1999**, *398*, 788–791.
(14) Hallbrucker, A.; Mayer, E.; Johari, G. P. *J. Chem. Phys.* **1989**, *93*, 7751–7752.
(15) Yue, Y.; Angell, C. A. *Nature* **2004**, *427*, 717–720.
(16) Minoguchi, A.; Richert, R.; Angell, C. A. *Phys. Rev. Lett.* **2004**, *93*, 215703/1–215703/4.
(17) Velikov, V.; Borick, S.; Angell, C. A. *Science* **2001**, *294*, 2335–2338.
(18) McClure, S. M.; Safarik, D. J.; Truskett, T. M.; C Mullins, B. *J. Phys. Chem. B* **2006**, *110*, 11033–11036.
(19) Hansen, E. W.; Stolcker, M.; Schmidt, R. *J. Phys. Chem.* **1996**, *100*, 2195–2200.
(20) Morishige, K.; Nobuoka, K. *J. Chem. Phys.* **1997**, *107*, 6965–6969.
(21) Morishige, K.; Kawano, K. *J. Chem. Phys.* **1999**, *110*, 4867–4872.
(22) Schreiber, A.; Ketelsen, I.; Findenegg, G. H. *Phys. Chem. Chem. Phys.* **2001**, *3*, 1185–1195.

(23) Kittaka, S.; Ishimaru, S.; Kuranishi, M.; Matsuda, T.; Yamaguchi, T. *Phys. Chem. Chem. Phys.* **2006**, *8*, 3223–3231.
(24) Oguni, M.; Maruyama, S.; Wakabayashi, K.; Nagoe, A. *Chem. −Asian J.* **2007**, *2*, 514–520.
(25) Nagoe, A.; Kanke, Y.; Oguni, M. *J. Phys.: Condens. Matter* **2010**, *22*, 365105–365111.
(26) Castrillon, S. R.-V.; Giovambattista, N.; Aksay, I. A.; Debenedetti, P. G. *J. Phys. Chem. B* **2009**, *113*, 7973–7976.
(27) Preliminary result of the present work was reported inOguni, M.; Kanke, Y.; Namba, S. *AIP Conf. Proc.* **2008**, *982*, 34–38.
(28) Fujimori, H.; Oguni, M. *J. Phys. Chem. Solids* **1993**, *54*, 271–280.
(29) Oguni, M.; Matsuo, T.; Suga, H.; Seki, S. *Bull. Chem. Soc. Jpn.* **1977**, *50*, 825–833.
(30) Jana, S. K.; Mochizuki, A.; Namba, S. *Catal. Surv. Asia* **2004**, *8*, 1–13.
(31) Barrett, E. P.; Joyner, L. G.; Halenda, P. P. *J. Am. Chem. Soc.* **1951**, *73*, 373–380.
(32) Haida, O.; Matsuo, T.; Suga, H.; Seki, S. *J. Chem. Thermodyn.* **1974**, *6*, 815–825.
(33) Alcoutlabi, M.; McKenna, G. B. *J. Phys.: Condens. Matter* **2005**, *17*, R461–R524.
(34) Banys, J.; Kinka, M.; Macutkevic, J.; Völkel, G.; Böhlmann, W.; Umamaheswari, V.; Hartmann, M.; Pöppl, A. *J. Phys.: Condens. Matter* **2005**, *17*, 2843–2857.
(35) Johari, G. P. *Thermochim. Acta* **2009**, *492*, 29–36.
(36) Mazurin, O. V.; Startsev, Yu-K.; Stoljar, S. V. *J. Non-Cryst. Solids* **1982**, *52*, 105–114.
(37) Oguni, M. *J. Non-Cryst. Solids* **1997**, *210*, 171–177.
(38) Fujimori, H.; Oguni, M. *Solid State Commun.* **1995**, *94*, 157–162.
(39) Smirnov, P.; Yamaguchi, T.; Kittaka, S.; Takahara, S.; Kuroda, Y. *J. Phys. Chem. B* **2000**, *104*, 5498–5504.
(40) Osipov, Yu-A.; Zheleznyi, B. V. *Z. Fiz. Khim.* **1977**, *51*, 1264–1265.
(41) Stanley, H. E.; Teixeira, J. *J. Chem. Phys.* **1980**, *73*, 3404–3422.
(42) Sastry, S.; Debenedetti, P. G.; Sciortino, F.; Stanley, H. E. *Phys. Rev. E* **1996**, *53*, 6144–6153.
(43) Nagoe, A.; Kanke, Y.; Oguni, M.; Namba, S. *J. Phys.: Chem. B* **2010**, *114*, 13940–13943.
(44) Mallamace, F.; Branca, C.; Broccio, M.; Corsaro, C.; Mou, C.-Y.; Chen, S.-H. *Proc. Natl. Acad. Sci. U.S.A.* **2007**, *104*, 18387–18391.
(45) Angell, C. A. *J. Phys. Chem.* **1993**, *97*, 6339–41.
(46) Ito, K.; Moynihan, C. T.; Angell, C. A. *Nature* **1999**, *398*, 492–495.
(47) Faraone, A.; Liu, L.; Mou, C.-Y.; Yen, C.-W.; Chen, S.-H. *J. Chem. Phys.* **2004**, *121*, 10843–10846.